Unlocking the Potential of Pulsed Electrolysis: Mechanisms for Improved CO ₂ Electroreduction in GDE Systems

Butt, Esaar N.; Padding, Johan T.; Hartkamp, Remco

DOI
10.1021/acselectrochem.5c00264

Publication date
2025

Document Version
Final published version

Published in
ACS Electrochemistry

ACS Electrochemistry

Open Access

pubs.acs.org/electrochem

Article

Unlocking the Potential of Pulsed Electrolysis: Mechanisms for Improved CO_2 Electroreduction in GDE Systems

Esaar N. Butt, Johan T. Padding, and Remco Hartkamp*

Cite This: *ACS Electrochem.* 2025, 1, 2475−2483

Read Online

ACCESS | Metrics & More | Article Recommendations | Supporting Information

ABSTRACT: We demonstrate that pulsed electrolysis can unlock higher performance in CO_2 electroreduction (CO_2ER) on gas diffusion electrodes (GDEs), which we find are limited by cation-induced CO_2 depletion and reduced Faradaic efficiency (FE) at high cathodic potentials. Using continuum-scale modeling, we show that pulsing strategies significantly enhance current density compared to steady-state operation at the same mean potential. Thicker catalyst layers (CLs) particularly benefit from pulsed electrolysis, achieving higher current densities near the gas/liquid interface along with overall improvements in Faradaic and cathodic efficiency compared to constant-potential systems. This is caused by the prolonged time for the cations to transport back to and block the catalytic surface, which improves CO_2 accessibility. Tuning the pulse parameters, especially with unequal durations, results in a similar current density as a constant potential system, but with better Faradaic and cathodic efficiency. These findings underscore pulsed electrolysis as a scalable and effective method to enhance CO_2ER performance in GDE systems, offering practical improvements for industrial applications.

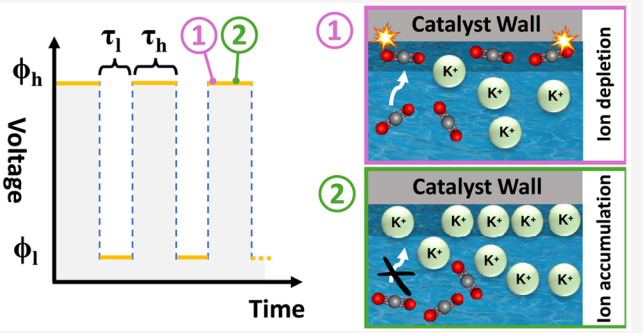

KEYWORDS: *Pulsed CO_2 Electrolysis, Gas Diffusion Electrodes, Pore Scale, Transient Mass Transport, Electric Double Layer, Size-modified Poisson Nernst Planck*

INTRODUCTION

The electrochemical reduction of CO_2 (CO_2ER) presents a promising avenue to mitigate CO_2 emissions while concurrently generating valuable chemical feedstocks and fuels.[1−4] Significant research efforts have been dedicated to scaling up CO_2ER to industrial levels,[5] with notable advances in catalyst development,[6] reactor design,[7] and process optimization.[8] Despite these advances, several challenges persist, including the need for high selectivity at industrial current densities and the reduction of energy consumption.[9] Configurations using gas diffusion electrodes (GDE) have shown great promise to overcome mass transfer limitations of dissolved CO_2 by positioning a porous catalyst layer (CL) between the gaseous CO_2 and the liquid electrolyte.

In addition to accessing the catalyst layer, the CO_2 must also reach the reaction plane. Our recent computational study of a liquid-filled GDE nanopore[10] has shown that excessive cation accumulation sterically hinders the access of CO_2 to the reaction plane at a high applied electrode potential, thus limiting the current density and Faradaic efficiency (FE). Moreover, another study postulated that the local current density in a GDE pore decreases with increasing distance from the gas/liquid interface due to CO_2 transport limitations into the liquid-filled pore.[11] A possible way to overcome this limitation is by periodically perturbing the reaction environment via an alternating electrode potential, known as pulsed electrolysis.[12,13] This technique has proven its ability in H-type cells to alter the selectivity of Cu and Ag catalysts through restructuring of the reaction environment,[14−16] and to enhance stability by mitigating restructuring of a Cu catalyst.[17,18] Combining the strengths of pulsing with those of a GDE configuration can be a powerful approach to leverage a high CO_2 transport rate while also having enhanced control over the local reaction environment within the porous matrix. Combining these techniques has been recently explored experimentally by Jeon et. al.[19] and by Li et al.,[20] who determined that pulsed operation can be used to tune the selectivity of C_1 and C_2 products in a GDE-type configuration. Recently, reverse-polarity pulsing has been shown to stabilize CO_2 to formate GDEs. Brief anodic segments periodically restored the GDE-based system, enabling sustained operation at high current densities.[21] Although experimental results have confirmed this to be a promising approach, experiments have

Received: June 27, 2025
Revised: October 7, 2025
Accepted: October 9, 2025
Published: October 18, 2025

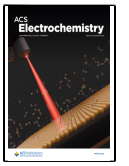

limited access to directly probe the high-resolution spatial and temporal concentration variations that would occur throughout the GDE during pulsed operation. In particular, experiments can only provide indirect insight into the fast electrical double-layer (EDL) response and the transport within the sub-micrometer pores of the catalyst layer. Therefore, pore-scale computational models are essential to obtain detailed insight into the evolving local reaction environment and ultimately to tailor the applied pulse to the specifics of the catalyst and operating conditions. To our knowledge, such a pore-scale model of pulsed CO_2ER in a GDE is currently lacking. Schröder et. al. developed a 1D GDE model to simulate pulsed current behavior for a metal-air battery system.[22] Some computational studies have focused on pulsed operation in CO_2ER, but again in the context of anH-cell configuration.[23,24] Heßelmann et.al. developed a 1D mass transport model for an Ag electrode accounting for the EDL formation and concluded that a pulsed operation increased current density and cathodic efficiency relative to a constant potential operation. However, their work does not answer the question whether pulsed operation would also benefit a GDE configuration operating at much higher (geometric) current densities.

In this work, we use time-dependent 2D continuum-scale simulations of a silver catalyst layer of a GDE to study mass transfer alongside the catalytic reactions that occur inside a GDE under pulsed electrolysis. We will demonstrate that pulsed electrolysis can help alleviate previously reported[10] steric and transport hindrances in a CL, resulting in an increase in the Faradaic and cathodic efficiency of the system relative to constant potential operation. We will establish that the Faradaic and cathodic efficiency can be modulated by adjusting the thickness of the CL, along with choosing a suitable pulse duration. We also propose a way to overcome the inefficient utilization of catalyst material in a GDE by leveraging pulsed electrolysis.

SIMULATION MODEL

Figure 1 shows a schematic representation of a GDE, where the zoomed-in part represents the 2D flooded pore space in the CL studied here. Gaseous CO_2 is introduced at the gas/liquid interface (boundary between gas diffusion layer and CL). It first dissolves in the electrolyte present inside the CL and then diffuses across the layer. CO_2 dissolution at the gas/liquid interface is governed by a film-theory-based boundary condition that accounts for resistance across an effective interfacial diffusion length appropriate to a flooded pore (see eqs 21 and 22 in the Supporting Information (SI)).[25] This parameter controls CO_2 entry into the electrolyte and is therefore critical for local CO_2 availability and Faradaic efficiency. Since the pore is completely flooded, the main mechanism of CO_2 transport considered in our work is molecular diffusion. The flowing bulk electrolyte is present at the end of the CL ($x = L$). CO_2 gets reduced at the catalyst surface. The simulation domain in radial direction extends from CL centerline at R = 0 to the Outer-Helmholtz-Plane (OHP) (R = 5 nm). Consistent with the Gouy-Chapman-Stern picture and prior pore-level CO_2ER models,[26−28] we use the OHP as the interfacial reference for the Frumkin-corrected kinetics: the driving force is the metal−OHP potential difference, and reactant activities are evaluated at the OHP. Catalyst-specific interfacial behavior is treated implicitly through the apparent kinetic parameters. The main CO_2ER product for the polycrystalline Ag surface considered here is

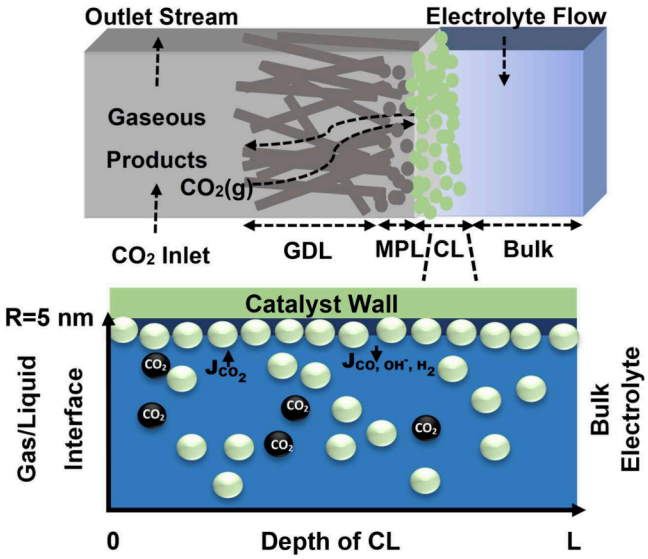

Figure 1. Schematic of a typical gas diffusion electrode. The zoomed-in section highlights the pore space in the catalyst layer (CL) with a characteristic depth L and characteristic radius R. Note that this schematic is not to scale because typically $L \gg R$.

CO. The model is adapted for a 0.1 M $KHCO_3$ solution and resolves the electric potential and concentration profiles of all solution species inside the CL pore space. Mass transfer is modeled using the size-modified Poisson-Nernst-Planck (SMPNP) equations[10,29−34] and the Frumkin-corrected Tafel equations are used to model the electrochemical reactions.[26,35−38] While kinetics are parameterized here for polycrystalline Ag, the modeling framework is readily extendable to other catalysts. For example, a Cu-based kinetic scheme can be implemented at the reaction boundary to capture both C1 and C2 product pathways, while the underlying SMPNP transport equations remain unchanged. The finite element package FEniCS is used to solve the weak formulation of the nonlinear SMPNP equations. Temporal discretizations are carried out using the backward Euler scheme, with a time step of 10^{-6} s. A variable mesh spacing is used in the simulation domain, with a finer mesh near the high-potential boundaries. Details of the model and all relevant boundary conditions are provided in the SI.

In this study, we focus on rectangular pulsed potential operations. A high cathodic potential Φ_h is applied for a duration of τ_h, after which a lower cathodic potential Φ_l is applied for a duration τ_l, and the process repeats. Although the cathodic potential is applied homogeneously along the catalyst surface (high solid conductivity), the resulting partial current densities will vary both in time and space due to the locally varying concentrations of reactive and charged species. Such local insight and control over conditions are instrumental in better understanding how to optimize electrochemical cells, but they are largely inaccessible in experiments. We will present both local and spatially averaged current densities to analyze overall performance and explain the causes of this performance.

RESULTS

Figure 2a shows the applied pulsed potential profile for a CO_2ER system, with the resulting partial current density shown in Figure 2b. For this study, the system is pulsed

https://doi.org/10.1021/acselectrochem.5c00264
ACS Electrochem. 2025, 1, 2475−2483

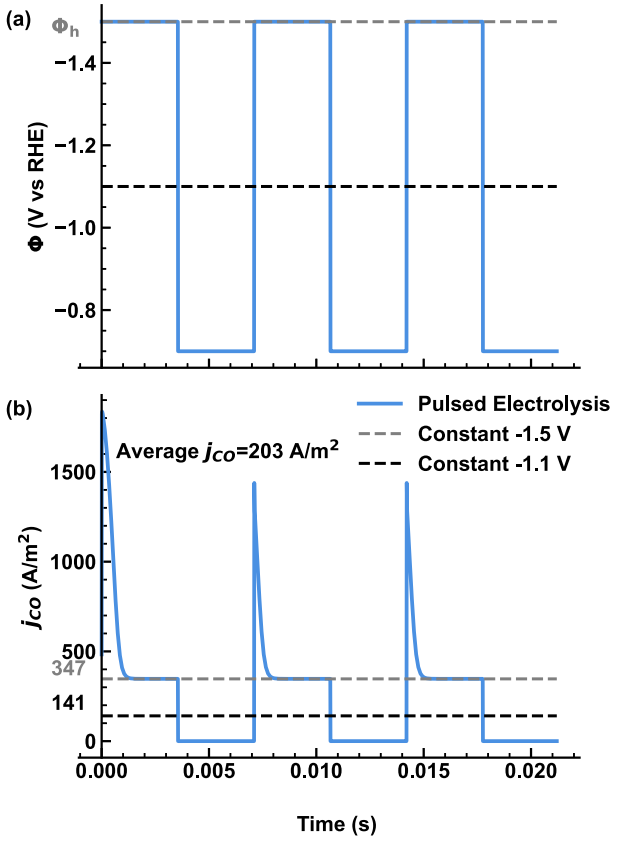

Figure 2. (a) Pulsed potential profile for a 200 nm thick CL. The black dotted line represents the mean potential of the pulsed operation. (b) Corresponding current density of CO_2 conversion to CO (j_{CO}), averaged over the length of the pore. Dotted lines correspond to the j_{CO} values for the constant potential operations.

between Φ_h = −1.5 and Φ_l = -0.7 V vs RHE. Φ_h = −1.5 V is sufficiently cathodic to drive CO_2ER on Ag without the pronounced loss of CO selectivity and parasitic HER that occur at more negative potentials, while Φ_l = −0.7 V (near the Ag PZC) allows interfacial relaxation and CO_2 replenishment between pulses. This range thus provides suitable conditions for achieving high selectivities toward the desired CO_2ER reaction. The reaction rate at Φ_l is negligible (Figure 2b), such that the CO_2ER occurs predominantly during the Φ_h phase of the pulse period. In conjunction with the low consumption of CO_2 during the Φ_l phase, there is a decrease in the concentration of electrostatically accumulated cations at the reaction plane. Together, this enables replenishing of the CO_2 concentration inside the pore space, such that the next pulse cycle again starts with a high current density. However, the CO_2 concentration does not completely return to the uniform concentration distribution at which the simulation began. Consequently, the first current density (j_{CO}) peak in Figure 2b) is not representative of the periodic process, and this peak will henceforth be omitted from the analysis.

Benchmark Case. We will first analyze a benchmark case, in which the thickness of the CL is L = 200 nm, the pore radius is R = 5 nm, and the durations of the pulse spent at Φ_h and Φ_l are equal, $\tau_h = \tau_l$ = 3.5 ms. In the later sections, we will also consider the implications of an unequal τ_h and τ_l and the influence of varying the thickness L of the CL on the performance of a pulsed system. The values for τ_h and τ_l in the benchmark case are based on the approximate time needed to reach a steady state in similar GDE geometries.[10] We will show later that this relaxation time increases with the CL thickness. Correspondingly, most experimental explorations of pulsed electrolysis involve longer pulses, because the typical experimental CL thickness is also larger than those considered here. Our purpose is not to mimic an entire experimental CL, but rather to provide mechanistic insights into how transport limitations and non-uniform concentrations within the CL fundamentally influence performance, revealing the critical roles of CL thickness and pulsing frequency. These insights can inform and guide the interpretation and optimization of experimental systems.

We first demonstrate the utility of pulsed electrolysis by comparing the time-averaged current density and Faradaic efficiency values obtained from a CO_2ER system under pulsed operation with those obtained from a system operating under a constant benchmark applied potential. One option for this benchmark potential is a constant potential operation at the same voltage efficiency ($\frac{\Phi^0}{\Phi_m}$). This corresponds to the mean potential of the pulsed system (Φ_m = −1.1 V), represented by the black dotted line in Figure 2a. Alternatively, the time-averaged current density and Faradaic efficiency can be compared to those of a system operating at a constant potential of Φ_h (−1.5 V) (gray line in Figure 2a). The time-averaged current density (j_{CO}) achieved through pulsed operation is 203 A/m^2. This is ≈ 44% higher than for a system operating at a constant applied potential of −1.1 V, due to a combination of the transient high current densities at the beginning of the Φ_h section of the pulse cycle, followed by a steady j_{CO} that is more than twice as high as the current density of a system operating at constant −1.1 V. During the Φ_l section of the pulse, the reaction rate of CO_2ER will initially be lower than that of HER due to CO_2 deficiency at the OHP (Figure S11). As the CO_2 concentration gradually replenishes near the OHP, the gap between the reaction rates for both catalytic reactions decreases. The time-averaged j_{CO} = 203 A/m^2 of a pulsed system is ≈41% lower than j_{CO} of a system operating continuously at a potential of Φ_h (Figure 2b). Despite the higher time-averaged j_{CO} of the pulsed system compared to the constant -1.1 V operation, Figure 3 shows that the pulsed system has a lower Faradaic efficiency toward CO production, due to the exponential potential dependence of the competing HER, with half of the cycle spent at the more

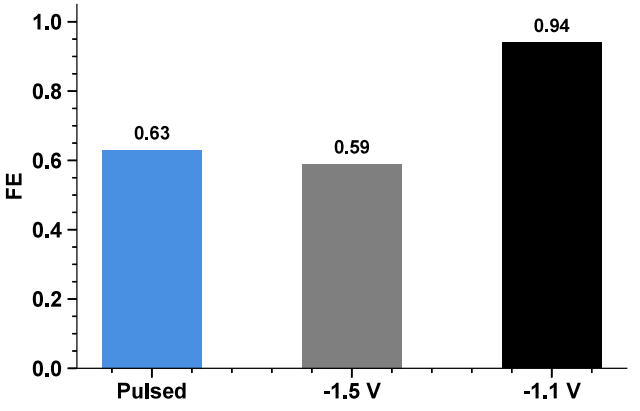

Figure 3. Faradaic efficiencies for a 200 nm thick CL under pulsed operation (Φ_h = −1.5 V, Φ_l = −0.7 V, $\tau_h = \tau_l$ = 3.5 ms.) and with constant potentials of −1.1 V and −1.5 V.

https://doi.org/10.1021/acselectrochem.5c00264
ACS Electrochem. 2025, 1, 2475−2483

cathodic Φ_h. In contrast, an ≈ 4% increase in selectivity towards CO is observed in a pulsed operation compared to a system operation at a constant -1.5 V potential. This increase is largely due to the transient high current densities observed in the Φ_h phase of the pulse, as illustrated in Figure 2b.

To fully appreciate the strength of applying pulsed electrolysis with a gas diffusion electrode, it is important to understand the spatial variations across the CL. Figure 4 shows

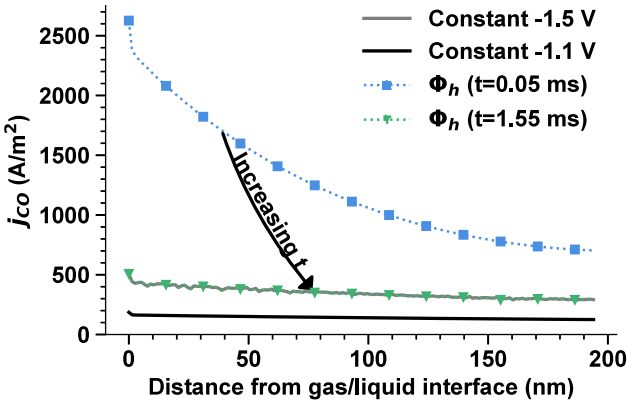

Figure 4. Local current density against the distance from the gas/liquid interface in a 200 nm thick CL for pulsed electrolysis (Φ_h = −1.5 V, Φ_l = −0.7 V, $\tau_h = \tau_l$ = 3.5 ms) at different times compared to the current density profile of systems operating at constant potentials of −1.1 V and −1.5 V.

that the previously discussed peak in current density directly after the onset of Φ_h can be largely ascribed to the region near the gas/liquid interface, where the local transient current density is up to five times its steady-state value. The high current densities decay to a state that maintains some of its spatial variation. This decay is due to two concurrent mechanisms: In the first place, CO_2 at the catalyst surface is consumed faster than it is supplied from the gas/liquid interface. Second, as more cations migrate from the bulk reservoir into the CL, their accumulation at the OHP sterically hinders the remaining CO_2 molecules. The competition between transport and consumption rates suggests a strong dependence of both the local and global current density on the thickness of the CL.

Influence of CL Thickness. It is clear from the above analysis that the time spent in the transient state is critical to control the performance of pulsed electrolysis. This transient time depends on the transport time scales in the CL, which in turn are affected by the pore length and radius. Because of the high aspect ratio of the pore, its length will be decisive for the duration of the transient. Therefore, we compare the current density profile under pulsed electrolysis for 100-400 nm thick CLs (Figure 5a), applying the same potential range and pulse duration as in the previous simulations. It can be observed that the decay time of the current density from its initial peak to a steady value increases almost linearly with the CL thickness, as shown in Figure 5b, whereas the peak height and the steady-state current density decrease with increasing CL thickness. This leads to an overall drop in average current density with an increase in CL thickness (Figure 5c), but this decrease is less severe in pulsed electrolysis compared to constant potential operation. Moreover, the current densities are achieved with higher cathodic efficiency in pulsed operation ($\frac{\Phi_0}{\Phi_m}$·FE) (Figure

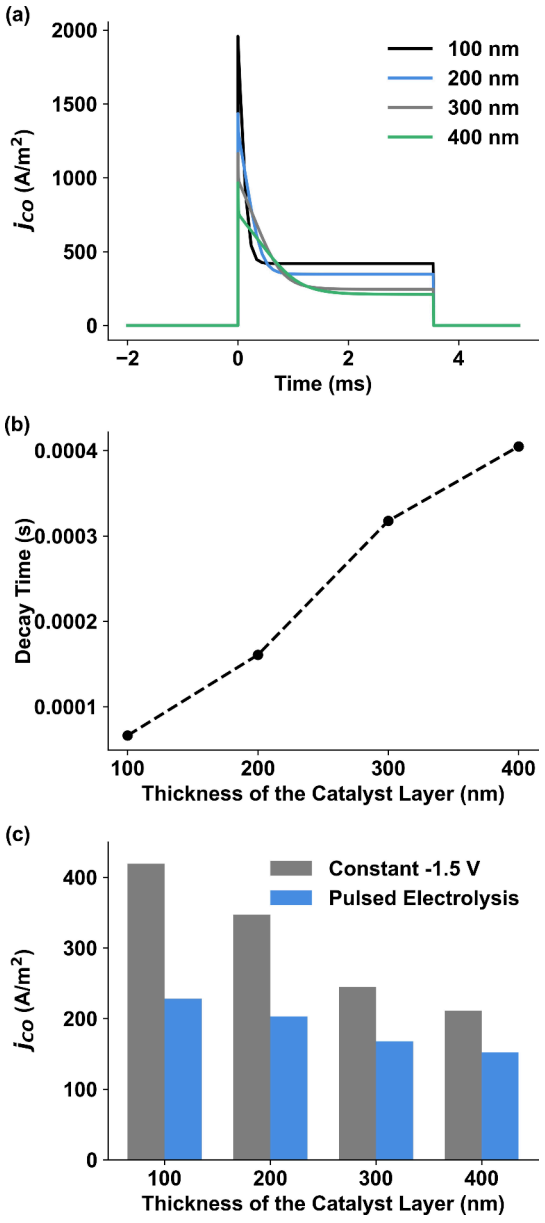

Figure 5. (a) j_{CO} profile with time for an Ag polycrystalline GDE system under pulsed electrolysis for varying thicknesses of CL. (b) Variation of j_{CO} decay time with changing thickness of the CL. (c) Comparison of absolute j_{CO} between a constant potential operation at −1.5 V and pulsed electrolysis, for various thicknesses of the CL. Φ_h = −1.5 V, Φ_l = −0.7 V, $\tau_h = \tau_l$ = 3.5 ms.

S8). Importantly, the drop only applies to spatially averaged current densities. In contrast, the local transient current densities near the gas/liquid interface are initially higher for the thicker CLs, and they endure for longer, eventually decaying to a lower steady-state value (Figure S2). All of these observations are a result of mass transport limitations, as we will demonstrate in the following.

Figure 6a shows the CO_2 concentration along the OHP up to the first 100 nm from the gas/liquid interface for a 200 nm and a 400 nm thick CL. Both CLs show a monotonic decrease in CO_2 concentration away from the gas/liquid interface and a drop in concentration with time. The higher CO_2 concentrations in the 400 nm thick CL, compared to the 200 nm thick CL, facilitate the higher local transient current densities in the

https://doi.org/10.1021/acselectrochem.5c00264
ACS Electrochem. 2025, 1, 2475−2483

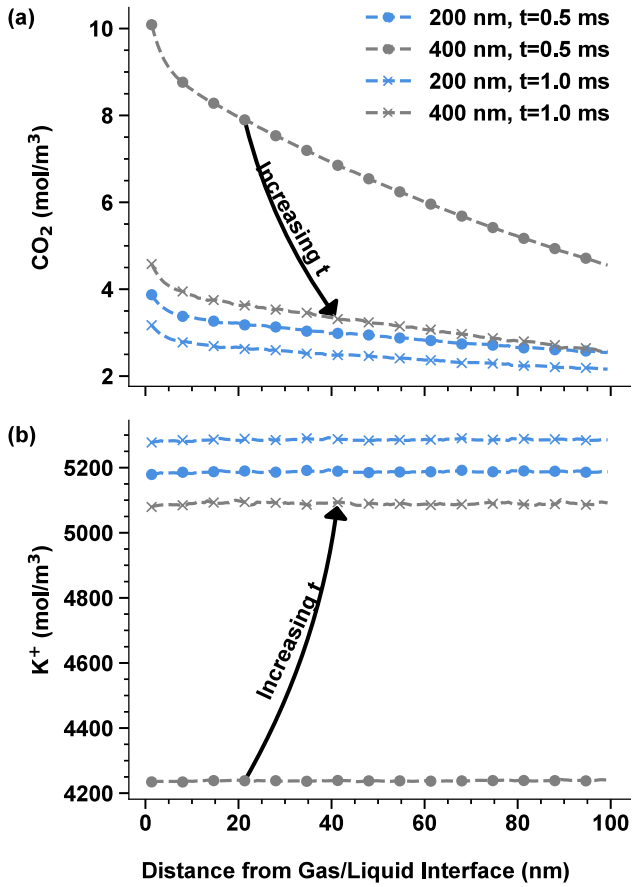

Figure 6. CO_2 (a) and K^+ (b) concentration profiles along the OHP up to 100 nm away from the gas/liquid interface for CL thicknesses of 200 and 400 nm at different times during the Φ_h section of the pulse cycle, $\Phi_h = -1.5$ V, $\Phi_l = -0.7$ V, $\tau_h = \tau_l = 3.5$ ms.

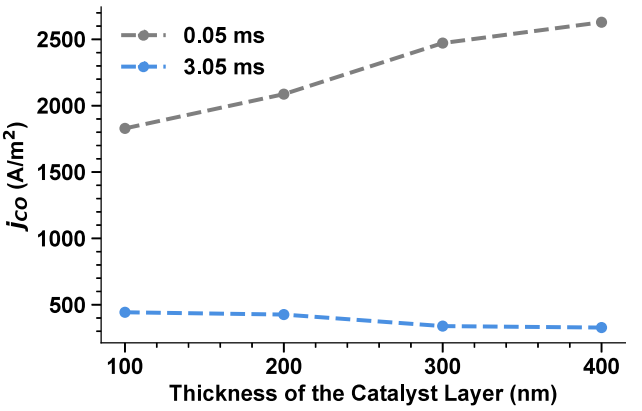

Figure 7. Local j_{CO} at a location 15 nm away from the gas/liquid interface for 100-400 nm thick CLs at different times. $\Phi_h = -1.5$ V, $\Phi_l = -0.7$ V, $\tau_h = \tau_l = 3.5$ ms.

thicker CL. Despite the corresponding higher CO_2 consumption rate, the 400 nm CL retains a higher local CO_2 concentration at the reaction plane than the 200 nm CL at least up to 1 ms after the onset of Φ_h. Consequently, the 400 nm thick CL would also retain a higher local current density than the 200 nm. Notably, the spatially-averaged current density 1 ms after the onset of Φ_h was found to be lower (Figure 5a) for the 400 nm CL than for the 200 nm CL.

The main reason for the difference in CO_2 concentration between the two catalyst layers during the transient regime is the difference in the amount of steric hindrance posed by cations at the OHP (Figure 6b). The inverse relation between the cation concentration and the presence of CO_2 molecules near the OHP has been extensively documented in previous works, where only constant potential operation was considered.[10,27] Pulsed operation has the potential to temporarily mitigate the detrimental effect of steric hindrance on CO_2ER by leveraging the finite transport time of the cations. This suggests that thicker CLs are beneficial to the transient local current density near the gas/liquid interface, which is farthest from the bulk electrolyte and nearest to the CO_2 supply. This is confirmed in Figure 7, which shows that j_{CO} 15 nm away from the gas/liquid interface shortly after the onset of Φ_h (t = 0.05 ms) increases with the thickness of the CL. After 3.05 ms, the transient advantage has vanished and the steady local current density has become nearly the same for each of the CL thicknesses considered here, in contrast to the pore-averaged steady-state current densities (Figure 5a).

Based on these findings, one can leverage the benefits of CL thickness and pulsed operation by designing a porous layer with a spatially varying catalyst loading. Experiments with gradient catalyst loading have demonstrated that just adding more catalyst does not ensure better performance, since this would also require more CO_2 to be transported to the catalyst surface.[39] Alternatively, suppose that the active catalyst material is only present near the gas/liquid interface. In that case, the CO_2 only faces a short transport path, whereas the remainder of the porous layer prolongs cationic transport. Under these conditions, the pore-averaged current densities for pulsed and constant potential operations will be in line with the local current densities depicted in Figure 7. For such a system, the current density would be significantly higher in a pulsed operation than in a constant potential operation, and the transient current density would increase with CL thickness. Figure S2 shows that the local current densities increase with the thickness of the CL up to the first 45 nm away from the gas/liquid interface. Hence, this could serve as a cut-off length for the active CL.

Interestingly, immediately after the onset of Φ_h, the concentration of cations near the gas/liquid interface exhibits a non-monotonic temporal trend, which is not seen for the cation concentration near the electrolyte reservoir (Figure S12). This is consistent with the relatively slow screening of the electric potential near the gas/liquid interface (Figure S7). The double-layer charging will cause a rapid drop in the cation concentration in the center of the pore, driving a flux of additional cations from the electrolyte reservoir into the pore until a new steady state has formed. These two steps are characterized by a separation time scale for the region near the gas/liquid interface, whereas the region closest to the electrolyte reservoir has readily available cations. The cation concentration along the centerline of the pore (in Figure S12) shows the highest value 10 nm away from the gas/liquid interface after 10^{-5} s. The migratory flux dominates the diffusive forces at this stage, leading to a net accumulation of cations and a depletion of anions near the gas/liquid interface. This causes a charge imbalance even at the center of the CL, despite the 5 nm pore radius being 5 times larger than the Debye length corresponding to the 0.1 M bulk electrolytic concentration. To quantify the competing fluxes for a 400 nm

https://doi.org/10.1021/acselectrochem.5c00264
ACS Electrochem. 2025, 1, 2475−2483

thick CL, the ratio of migratory flux (J_{mig}) to diffusive flux (J_{diff}) can be expressed as $\frac{J_{mig}}{J_{diff}} = \frac{C_{K,avg}}{\Delta C_K}\left(\frac{\Delta\phi}{V_{ther}}\right)$. At $t \sim 10^{-5}$ s, the average K^+ concentration along the centerline of the pore is approximately $C_{K,avg}$ = 125 mol/m^3, the concentration difference is ΔC_K = 170 mol/m^3, and the normalized potential difference is $\Delta\phi/V_{ther}$ = 2. The value for $\frac{J_{mig}}{J_{diff}}$ is ≈ 1.5 at $t \sim 10^{-5}$ s. Over time, as the electric field stabilizes and approaches bulk values, the flux ratio decreases, reducing the concentration gradient between the bulk phase and the gas/liquid interface (as seen at $t \sim 10^{-4}$ s in Figure S12). By $t \sim 10^{-3}$ s, the cations near the OHP have reached the steric crowding limit, leading to a subsequent thickening of the cation layer. This results in the final observed increase in the cation concentration at the center of the CL.

This dynamic interplay between migration and diffusion highlights the transient and spatially dependent nature of ion transport in catalyst layers. Importantly, this challenges the widely used assumption of electroneutrality, which is rarely valid inside these narrow catalyst layers at any time during the process. The deviations from electroneutrality are significant and persist throughout the system, influencing the overall ion transport dynamics and concentration profiles.

Influence of Pulse Duration. Until now, we have discussed how the CL thickness affects the performance of pulsed electrolysis in a GDE. The performance can be further improved by tuning the pulse duration (τ_h, τ_l) and the upper and lower bounds of the applied potential (Φ_h, Φ_l). In Figure 8, the black line shows the j_{CO} profile obtained using the same

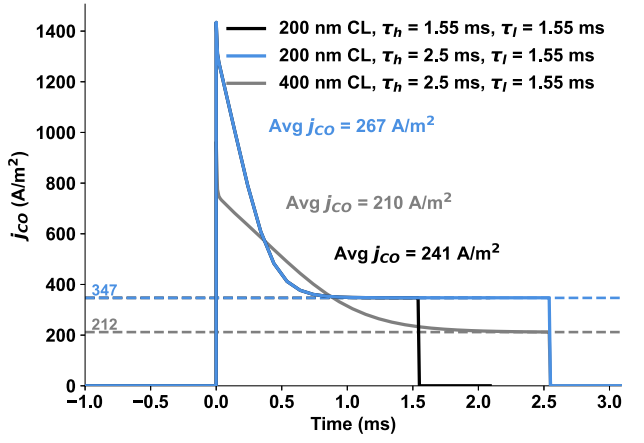

Figure 8. Comparison of j_{CO} between pulsed electrolysis and a constant potential operation of −1.5 V at varying operating conditions for Φ_h = −1.5 V and Φ_l = −0.7 V.

Φ_h and Φ_l values as in Figure 2, but with each half-cycle shortened to 1.55 ms instead of 3.5 ms. The shorter τ_h reduces the time spent at the steady state plateau, thereby making better use of the transient regime. Although the time averaged j_{CO} remains lower than that of a constant-potential system, the gap is markedly smaller than in the longer pulse case of Figure 2b. Likewise, the reduced τ_l shortens the duration of the low-CO_2ER phase.

The pulse profile can be further optimized by applying Φ_h and Φ_l for unequal durations. In Figure 8, the blue line (unequal durations, τ_h = 2.5 ms, τ_l = 1.55 ms) yields a higher time-averaged j_{CO} compared to the black line (equal durations, τ_h = τ_l = 1.55 ms). However, the mean potential of the unequal-duration pulse is ≈ −1.2 V, compared to −1.1 V for the equal-duration case, indicating that the increase in current density comes at the expense of lower voltage efficiency.

As shown earlier in Figure 5c, increasing the catalyst layer thickness reduces the difference in j_{CO} between pulsed and constant potential systems when Φ_h = Φ_l. Applying unequal pulse durations to a thicker CL further minimizes this difference. In Figure 8, the grey line (τ_h = 2.5 ms, τ_l = 1.55 ms, 400 nm CL) illustrates that the time-averaged j_{CO} of the periodic pulse nearly matches that of the constant potential case, while operating at a higher cathodic efficiency (Figure S9). Figure 9a compares the time-averaged current density for

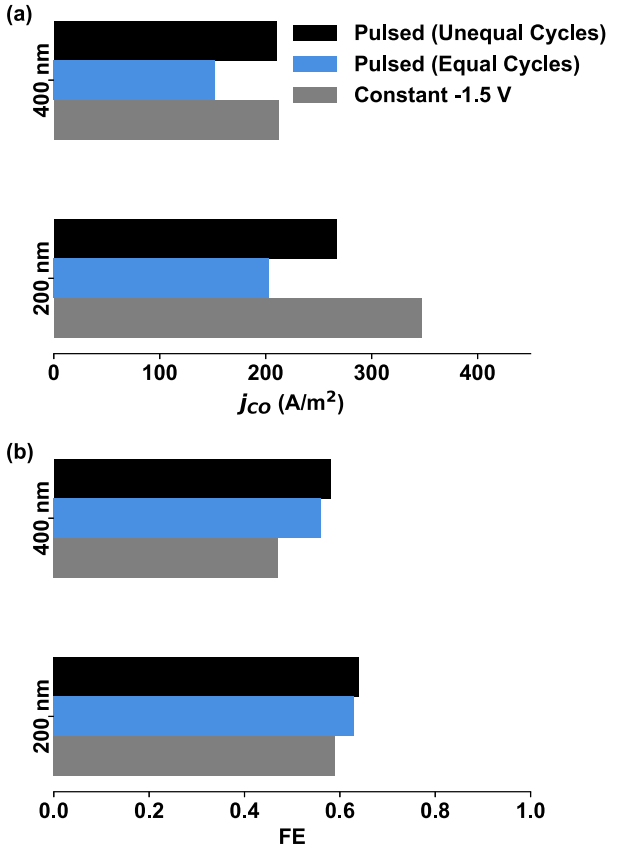

Figure 9. Comparison of constant potential operation of −1.5 V, pulsed electrolysis with equal cycles (τ_h = τ_l = 3.5 ms) and pulsed electrolysis for unequal cycles (τ_h = 2.5 ms, τ_l = 1.55 ms) for 200 and 400 nm thick CL, (a) j_{CO}, (b) FE.

a system operating at a constant potential to that for pulsed systems at both equal and unequal τ_l and τ_h. The data show that the lower current density in pulsed operation compared to constant potential operation can be remedied by unequal pulsing, even resulting in a negligible difference between constant potential and pulsed operation for the 400 nm CL. The Faradaic efficiency is higher for each of the pulsed operation systems studied here (Figure 9b). However, the gain is again higher when $\Phi_h \neq \Phi_l$ and for the thicker CL. Naturally, the unequal mode corresponds to a higher mean potential relative to the equal-mode operation; hence, there will be a drop in cathodic efficiency, but it remains higher than that of the constant potential system (Figure S9). Thus, for a larger CL, the operating parameters of pulsed electrolysis can

https://doi.org/10.1021/acselectrochem.5c00264
ACS Electrochem. 2025, 1, 2475−2483

be tuned to give better FE results at a higher cathodic efficiency compared to constant potential operation without compromising the current density of CO_2ER.

DISCUSSION

The duration of application for Φ_h and Φ_l is critical for optimizing the performance of pulsed electrolysis in a GDE. The suitable choice for τ_l depends on the CO_2 replenishing time, which in turn depends on the thickness of CL. In this work, a minimum τ_l = 1.5 ms was sufficient to replenish the concentration of CO_2 in each of the catalyst layers studied. The benefits of transient current density can be optimally leveraged if τ_h is similar to the decay time of the j_{CO}. A τ_h higher than the decay time would diminish the transient gains in FE, whereas lowering it will decrease the time-averaged j_{CO}. Notably, the decay time could be several orders of magnitude larger (of the order of a few seconds) in a planar electrode assembly due to increased mass transport limitations. As Figure 5b showed, the decay time for current density increases linearly with increasing catalytic layer thickness. Hence, a suitable τ_h can be inferred based on the thickness of the GDE CL. Operationally, the model can be used to define the current decay time at a selected Φ_h as the time required for j_{CO} to reach its steady value after stepping from Φ_l to Φ_h. This sets the $\tau_h \approx t_{\text{decay}}(L)$. The CO_2 replenishment time τ_l at Φ_l can analogously be evaluated as the time for the interfacial CO_2 concentration to return to its steady value. Once τ_h and τ_l are determined, if current density is prioritized, one can modestly increase τ_h while maintaining τ_l so that replenishment is not compromised. At high pulsing rates, the energy associated with capacitative charging during each cycle can become prohibitive. This capacitive energy reduces the energy efficiency and is dissipated as heat. This effect is not considered here because the pulsing rates in practical applications will be much lower than those for the thin CLs studied here.

As a continuum treatment, the model does not resolve the Stern layer; thus, effects such as specific adsorption, short-range interactions, and molecular orientation are absorbed into apparent kinetic parameters. These effects have previously been shown to influence the stabilization of reaction intermediates, which influences product selectivity, especially for CO_2ER processes that focus on C_{2+} products.[40,41] Capturing these effects more faithfully will require coupling pore-scale transport to explicit multistep surface kinetics[42] and/or particle-based interfacial models. Future modeling approaches should incorporate microkinetic models to accurately determine the influence of intermediate species on product selectivities.[24] Pulsed electrolysis also affects the pH behavior inside the CL, as illustrated in Figure S6; a more detailed analysis of how these pulse-induced pH variations influence the interfacial kinetics (through stabilization of intermediates) will be considered in future extensions of this model. Another possible application of pulsed electrolysis is the alleviation of local gas supersaturation during low potential intervals, temporarily restoring interfacial mass transfer as observed in similar gas-evolving electrodes;[43] however, confirming this effect would require detailed bubble nucleation modeling.

In this work, the CL was represented by a uniform cylindrical pore of fixed radius, whereas in reality, catalyst layers consist of a distribution of pore sizes and morphologies. Another natural extension of the present framework is to develop pore network models, which would capture this heterogeneity and allow systematic evaluation of how pore size distributions impact local transport, reaction environments, and overall GDE performance.

Although the current densities predicted by our model are entirely associated with the Faradaic reactions, capacitive charging can be predicted based on electrical double layer theory. For a 200 nm thick CL, $W = \frac{1}{2}C\Delta\Phi_m^2 \approx 5\mu\text{J/cm}^2$ per pulse cycle. This is 40 times smaller than the energy that goes into the CO_2ER reaction (for $\tau_h = \tau_l$ = 3.5 ms). For the GDE geometry under consideration, the time constant for the decay of the capacitative current density is only a few nanoseconds, $T = \lambda_d R/D$. Here, λ_d is the Debye length, R is the radius of a pore in the CL, and D is the diffusion coefficient of the dominant cation (in this case potassium). This is also in accordance with EDL equilibration times found in molecular dynamic simulations.[44] This capacitive time is extremely short compared to τ_h in our pulse model. Additionally, the ability to sustain high-frequency pulsing rates is contingent on the chemical and physical properties of the catalytic system, but also on the performance of the associated power electronics. Power electronics must be capable of rapidly switching potentials without significant losses or inefficiencies, which can pose a challenge at these time scales. Future studies could explore the interplay between power electronics performance and reaction efficiency, as well as the associated energy costs for different switching regimes.

CONCLUSION

We conducted simulations to investigate the behavior of a GDE-based polycrystalline Ag CO_2ER system under pulsed electrolysis. To analyze the performance, we compared the current density and FE attained under pulsed operation with a system under the application of a constant potential. Pulsed electrolysis was shown to yield a significant increase in j_{CO} compared to the mean potential due to the transient high current densities during the Φ_h part of the pulse. The FE, however, drops significantly because the rate of HER increases exponentially with potential. When comparing the performance of pulsed electrolysis with a system under a constant high potential of -1.5 V (Φ_h), we observed a 41% drop of j_{CO} and an ≈4% increase in FE of CO_2ER reaction.

We determined that the relative performance of a pulsed system is intricately linked to the time spent in the transient current density state, with a longer transient leading to improved Faradaic and cathodic efficiencies. This transient state can be prolonged by increasing the thickness of the catalyst layer as a result of the increased time for the cationic transport. This directly influences the CO_2 concentration at the OHP due to less steric hindrance. We also observed that the current density near the gas/liquid interface increases with CL thickness. Based on this, we recommended applying a catalytically active CL only until a certain distance, maximizing the current density while reducing the catalyst cost. This study also shows that transient cation accumulation near the gas/liquid interface leads to substantial deviations from electroneutrality, challenging widely held assumptions in catalyst layer modeling and affecting overall ion transport. We further determined that tuning the time for each part of the pulse (τ_h vs. τ_l) also leads to improved performance. A shorter pulse with unequal duration ($\tau_h > \tau_l$) performed better than an equal duration pulse. Both equal and unequal pulses lagged in terms of j_{CO} compared to a constant potential operation for a 200 nm

https://doi.org/10.1021/acselectrochem.5c00264
ACS Electrochem. 2025, 1, 2475−2483

thick CL. For a 400 nm thick CL, a shorter unequal pulse resulted in a similar j_{CO} as a system under constant potential at a higher cathodic efficiency. Furthermore, both equal and unequal pulses resulted in increased FE for CO_2ER, with unequal pulses outperforming the equal pulsed operation. We also showed that τ_h can be selected based on the decay time for j_{CO}. The decay time increases almost linearly with the increase in the thickness of the CL. This is especially helpful for researchers working with varying thicknesses of the CL.

The analysis provided in this study proves that pulsed electrolysis can be extremely beneficial for GDE-based CO_2ER systems, especially for thicker catalyst layers. These findings can also benefit the improvement of other electrochemical reduction processes that use gas diffusion electrodes. Future research should focus on optimizing the duration of each half of the pulse cycle for porous GDE systems.

■ ASSOCIATED CONTENT

Supporting Information

The Supporting Information is available free of charge at https://pubs.acs.org/doi/10.1021/acselectrochem.5c00264.

Extensive overview of transport-related equations, boundary conditions, and modeling parameters used in this work, as well as additional results (PDF)

■ AUTHOR INFORMATION

Corresponding Author

Remco Hartkamp − *Department of Process and Energy, e-Refinery Institute, and Process & Product Technology Institute (Pro2Tech), Delft University of Technology, Delft 2628 CB, the Netherlands;* orcid.org/0000-0001-8746-8244; Phone: +31 15 27 86674; Email: r.m.hartkamp@tudelft.nl

Authors

Esaar N. Butt − *Department of Process and Energy, e-Refinery Institute, and Process & Product Technology Institute (Pro2Tech), Delft University of Technology, Delft 2628 CB, the Netherlands;* orcid.org/0000-0002-5050-7649

Johan T. Padding − *Department of Process and Energy, e-Refinery Institute, and Process & Product Technology Institute (Pro2Tech), Delft University of Technology, Delft 2628 CB, the Netherlands;* orcid.org/0000-0003-4161-0748

Complete contact information is available at: https://pubs.acs.org/10.1021/acselectrochem.5c00264

Notes

The authors declare no competing financial interest.

■ ACKNOWLEDGMENTS

This work is part of the research program Towards large-scale electroconversion systems (TOeLS) financed by Shell and the Topsectors Chemistry, HTSM and Energy.

■ REFERENCES

(1) Yan, Z.; Hitt, J. L.; Turner, J. A.; Mallouk, T. E. Renewable electricity storage using electrolysis. *Proc. Natl. Acad. Sci. U.S.A.* **2020**, *117*, 12558−12563.

(2) Lu, X.; Leung, D. Y.; Wang, H.; Leung, M. K.; Xuan, J. Electrochemical Reduction of Carbon Dioxide to Formic Acid. *ChemElectroChem.* **2014**, *1*, 836−849.

(3) Resasco, J.; Chen, L. D.; Clark, E.; Tsai, C.; Hahn, C.; Jaramillo, T. F.; Chan, K.; Bell, A. T. Promoter Effects of Alkali Metal Cations on the Electrochemical Reduction of Carbon Dioxide. *J.Am.Chem.Soc.* **2017**, *139*, 11277−11287.

(4) Whipple, D. T.; Kenis, P. J. A. Prospects of CO_2 Utilization via Direct Heterogeneous Electrochemical Reduction. *J. Phys. Chem. Lett.* **2010**, *1*, 3451−3458.

(5) Masel, R. I.; Liu, Z.; Yang, H.; Kaczur, J. J.; Carrillo, D.; Ren, S.; Salvatore, D.; Berlinguette, C. P. An industrial perspective on catalysts for low-temperature CO_2 electrolysis. *Nat. Nanotechnol.* **2021**, *16*, 118−128.

(6) Li, F.; MacFarlane, D. R.; Zhang, J. Recent advances in the nanoengineering of electrocatalysts for CO_2 reduction. *Nanoscale* **2018**, *10*, 6235−6260.

(7) Ma, D.; Jin, T.; Xi, K.; Huang, H. An overview of flow cell architecture design and optimization for electrochemical CO_2 reduction. *J. Mater. Chem. A* **2021**, *9*, 20897−20918.

(8) Bhargava, S. S.; Proietto, F.; Azmoodeh, D.; Cofell, E. R.; Henckel, D. A.; Verma, S.; Brooks, C. J.; Gewirth, A. A.; Kenis, P. J. System Design Rules for Intensifying the Electrochemical Reduction of CO_2 to CO on Ag Nanoparticles. *ChemElectroChem.* **2020**, *7*, 2001−2011.

(9) Li, J.; Abbas, S. U.; Wang, H.; Zhang, Z.; Hu, W. Recent Advances in Interface Engineering for Electrocatalytic CO_2 Reduction Reaction. *Nano-Micro Lett.* **2021**, *13*, 216.

(10) Butt, E. N.; Padding, J. T.; Hartkamp, R. Local Reaction Environment Deviations within Gas Diffusion Electrode Pores for CO_2 Electrolysis. *J. Electrochem. Soc.* **2024**, *171*, 014504.

(11) Burdyny, T.; Smith, W. A. CO2 reduction on gas-diffusion electrodes and why catalytic performance must be assessed at commercially-relevant conditions. *Energy Environ. Sci.* **2019**, *12*, 1442.

(12) Casebolt, R.; Levine, K.; Suntivich, J.; Hanrath, T. Pulse check: Potential opportunities in pulsed electrochemical CO_2 reduction. *Joule* **2021**, *5*, 1987−2026.

(13) Liu, T.; Wang, J.; Yang, X.; Gong, M. A review of pulse electrolysis for efficient energy conversion and chemical production. *J. Energy Chem.* **2021**, *59*, 69−82.

(14) Shiratsuchi, R.; Aikoh, Y.; Nogami, G. Pulsed Electroreduction of CO_2 on Copper Electrodes. *J. Electrochem. Soc.* **1993**, *140*, 3479.

(15) Shiratsuchi, R.; Nogami, G. Pulsed Electroreduction of CO_2 on Silver Electrodes. *J. Electrochem. Soc.* **1996**, *143*, 582.

(16) Kim, C.; Weng, L.-C.; Bell, A. T. Impact of Pulsed Electrochemical Reduction of CO_2 on the Formation of C2. *Products over Cu. ACS Catal.* **2020**, *10*, 12403−12413.

(17) Jännsch, Y.; Leung, J. J.; Hämmerle, M.; Magori, E.; Wiesner-Fleischer, K.; Simon, E.; Fleischer, M.; Moos, R. Pulsed potential electrochemical CO2 reduction for enhanced stability and catalyst reactivation of copper electrodes. *Electrochem. Comm.* **2020**, *121*, 106861.

(18) Kok, J.; de Ruiter, J.; van der Stam, W.; Burdyny, T. Interrogation of Oxidative Pulsed Methods for the Stabilization of Copper Electrodes for CO_2 Electrolysis. *J.Am.Chem.Soc.* **2024**, *146*, 19509−19520.

(19) Jeon, H. S.; Timoshenko, J.; Rettenmaier, C.; Herzog, A.; Yoon, A.; Chee, S. W.; Oener, S.; Hejral, U.; Haase, F. T.; Cuenya, B. R. Selectivity Control of Cu Nanocrystals in a Gas-Fed Flow Cell through CO_2 Pulsed Electroreduction. *J. Am. Chem. Soc.* **2021**, *143*, 7578−7587.

(20) Li, Z.; Wang, L.; Sun, L.; Yang, W. Dynamic Cation Enrichment during Pulsed CO_2 Electrolysis and the Cation-Promoted Multicarbon Formation. *J. Am. Chem. Soc.* **2024**, *146*, 23901−23908.

(21) Bashir, S. M.; Gyenge, E. L. Improving the Stability of Gas Diffusion Electrodes for CO_2 Electroreduction to Formate with Sn and In-Based Catalysts at 500 mA cm^{-2}: Effect of Electrode Design and Operation Mode. *ACS Omega* **2025**, *10*, 1493−1509.

(22) Schroder, D.; Laue, V.; Krewer, U. Numerical simulation of gas-diffusion-electrodes with moving gas-liquid interface: A study on pulse-current operation and electrode flooding. *Comput. Chem. Eng.* **2016**, *84*, 217−225.

(23) Bui, J. C.; Kim, C.; Weber, A. Z.; Bell, A. T. Dynamic Boundary Layer Simulation of Pulsed CO_2 Electrolysis on a Copper Catalyst. *ACS Energy Lett.* **2021**, *6*, 1181−1188.
(24) Heßelmann, M.; Felder, D.; Plischka, W.; Nabi, S.; Linkhorst, J.; Wessling, M.; Keller, R. Dynamics of the Boundary Layer in Pulsed CO_2 Electrolysis. *Angew. Chem. Int. Ed.* **2024**, *63*, e202406924.
(25) El-Shafie, O. A.; El-Maghraby, R. M.; Albo, J.; Fateen, S.-E. K.; Abdelghany, A. Modeling and Numerical Investigation of the Performance of Gas Diffusion Electrodes for the Electrochemical Reduction of Carbon Dioxide to Methanol. *Ind. Eng. Chem. Res.* **2020**, *59*, 20929−20942.
(26) Butt, E. N.; Padding, J. T.; Hartkamp, R. Size-modified Poisson-Nernst-Planck approach for modeling a local electrode environment in CO_2 electrolysis. *Sustainable Energy Fuels* **2022**, *7*, 144−154.
(27) Bohra, D.; Chaudhry, J. H.; Burdyny, T.; Pidko, E. A.; Smith, W. A. Modeling the electrical double layer to understand the reaction environment in a CO_2 electrocatalytic system. *Energy Environ. Sci.* **2019**, *12*, 3380−3389.
(28) Johnson, E. F.; Boutin, E.; Liu, S.; Haussener, S. Pathways to enhance electrochemical CO_2 reduction identified through direct pore-level modeling. *EES Catalysis* **2023**, *1*, 704−719.
(29) Biesheuvel, P. M.; van Soestbergen, M.; Bazant, M. Z. Imposed currents in galvanic cells. *Electrochim. Acta* **2009**, *54*, 4857−4871.
(30) Bazant, M. Z.; Kilic, M. S.; Storey, B. D.; Ajdari, A. Towards an understanding of induced-charge electrokinetics at large applied voltages in concentrated solutions. *Adv. Colloid Interface Sci.* **2009**, *152*, 48−88.
(31) Kilic, M. S.; Bazant, M. Z.; Ajdari, A. Steric effects in the dynamics of electrolytes at large applied voltages. II. Modified Poisson-Nernst-Planck equations. *Phys. Rev. E Stat. Nonlin. Soft Matter Phys.* **2007**, *75*, 021502.
(32) Pilon, L.; Wang, H.; d'Entremont, A. Recent Advances in Continuum Modeling of Interfacial and Transport Phenomena in Electric Double Layer Capacitors. *J.Electrochem.Soc.* **2015**, *162*, A5158−A5178.
(33) Ringe, S.; Morales-Guio, C. G.; Chen, L. D.; Fields, M.; Jaramillo, T. F.; Hahn, C.; Chan, K. Double layer charging driven carbon dioxide adsorption limits the rate of electrochemical carbon dioxide reduction on Gold. *Nat. Commun.* **2020**, *11*, 33.
(34) Bohra, D.; Chaudhry, J. H.; Burdyny, T.; Pidko, E. A.; Smith, W. A. Mass transport in catalytic pores of GDE-based CO_2 electroreduction systems. *ChemRxiv*, 2020. DOI: 10.26434/chemrxiv.13073348.v1.
(35) Frumkin, A. wasserstoffuberspannung und struktur der doppelschicht. *Z. Phys. Chem.* **1933**, *164A*, 121−133.
(36) Rossi, M.; Wallmersperger, T.; Neukamm, S.; Padberg-Gehle, K. Modeling and Simulation of Electrochemical Cells under Applied Voltage. *Electrochim. Acta* **2017**, *258*, 241−254.
(37) Parsons, R. Structure of the electrical double layer and its influence on the rates of electrode reactions. *Advances in Electrochem. Electrochem. Eng.* **1961**, 1−64.
(38) Delahay, P. *Double Layer and Electrode Kinetics*, 2nd ed.; Interscience: 1965.
(39) Monteiro, M. C. O.; Dieckhöfer, S.; Bobrowski, T.; Quast, T.; Pavesi, D.; Koper, M. T. M.; Schuhmann, W. Probing the local activity of CO_2 reduction on gold gas diffusion electrodes: effect of the catalyst loading and CO_2 pressure. *Chem. Sci.* **2021**, *12*, 15682−15690.
(40) Casebolt, R.; Kimura, K. W.; Levine, K.; DaSilva, J. A. C.; Kim, J.; Dunbar, T. A.; Suntivich, J.; Hanrath, T. Effect of Electrolyte Composition and Concentration on Pulsed Potential Electrochemical CO_2 Reduction. *ChemElectroChem.* **2021**, *8*, 681−688.
(41) Kimura, K. W.; Casebolt, R.; DaSilva, J. C.; Kauffman, E.; Kim, J.; Dunbar, T. A.; Pollock, C. J.; Suntivich, J.; Hanrath, T. Selective Electrochemical CO_2 Reduction during Pulsed Potential Stems from Dynamic Interface. *ACS Catal.* **2020**, *10*, 8632−8639.
(42) Fan, R.; Habibi, P.; Padding, J. T.; Hartkamp, R. Coupling mesoscale transport to catalytic surface reactions in a hybrid model. *J. Chem. Phys.* **2022**, *156*, 084105.
(43) Zhang, S.; Cao, X.; Wang, B.; Wei, J.; et al. Application of high-frequency pulsed electrolysis technology in enhancing hydrogen production efficiency and energy saving potential analysis. *International Journal of Hydrogen Energy* **2025**, *109*, 684−693.
(44) Döpke, M. F.; Hartkamp, R. The importance of specifically adsorbed ions for electrokinetic phenomena: Bridging the gap between experiments and MD simulations. *J. Chem. Phys.* **2021**, *154*, 094701.